Complex photonic band diagrams for finite-size photonic crystals with arbitrary defects

Jiu Hui Wu, A. Q. Liu,[a] L. K. Ang, and T. H. Cheng
School of Electrical and Electronic Engineering, Nanyang Technological University, Singapore 639798, Singapore

K. Xu, J. Wu, and J. T. Lin
Key Laboratory of Optical Communication and Lightwave Technologies, Beijing University of Posts and Telecommunications, Beijing 100876, People's Republic of China

(Received 4 September 2006; accepted 4 January 2007; published online 1 March 2007)

Based on an effective propagation constant and a frequency-dependent dielectric constant, the plane wave method is extended to calculate the complex photonic band diagram and the density of states for electromagnetic waves propagating in a two-dimensional finite structure with nonoverlapping dielectric cylinders of arbitrary radii, which may be randomly embedded in a dielectric matrix. The effective propagation constant is obtained by using the Twersky formula [J. Math. Phys. **3**, 700 (1962)] and the scattering matrix method. A case study shows that an embedded defect with optimal radius in a finite photonic crystal can increase the first photonic band gap as compared to the similar structure without the defect. This work is expected to provide a useful tool in determining the photonic properties of a disorder dielectric medium with arbitrary embedded nanoparticles and nanowires. © *2007 American Institute of Physics*. [DOI: 10.1063/1.2696436]

I. INTRODUCTION

Photonic band structure refers to the propagation properties of electromagnetic waves travelling through a periodically modulated dielectric, which exhibits an absolute photonic band gap (PBG) that prohibits the propagation of light at any direction within a finite spectral range.[1] The photonic band diagram for infinite periodic photonic crystals can be calculated by using the conventional plane wave method (PWM).[2] However, any realistic photonic structure is finite, other than the ideal one, and the absolute band gap is not really necessary in realistic applications, in which a transmission of −60 dB (i.e., 0.001) to −40 dB (i.e., 0.01) is good enough to be considered as a band gap. Thus, it is of interest to calculate the photonic band diagram and the density of states of a finite photonic crystal with arbitrary defects. Many methods have been used to calculate the transmission of finite-size two-dimensional (2D) photonic crystals, such as the finite difference time domain (FDTD) method,[3,4] the scattering matrix method,[5,6] and the conventional PWM.[7] It is well known that the FDTD method can be applied for the band structure computations of finite periodic photonic crystals with artificial absorbing boundary conditions. In addition, the transfer-matrix method[8] can also be used by looking upon the photonic crystal as an infinite stack of identical periodic crystal layers along a certain direction. However, these are not the real conditions for realistic finite-size 2D photonic crystals, with or without defects.

Recently, the study of photonic band diagram and density of states (DOS) for a finite photonic structure is of considerable interest.[9–11] Both FDTD and finite element methods (FEM) are useful to calculate the transmission or reflection for finite PBG structure including the effects of boundary and defects. If they were used to create the photonic band diagram, some boundary conditions, such as perfectly matched layers, have to be followed artificially. In this paper, we introduce an accurate theoretical approach to calculate the complex photonic band diagram and the DOS of finite-size 2D circular cylinders, which are arbitrarily embedded in a dielectric matrix. From this model, it is possible to obtain an optimal setting of the finite structure according to the calculated complex band diagram, which can show light attenuation in the transmission along different directions. Some case studies will be presented.

The paper is organized as follows: the theory model is first presented in Sec. II, and the results and discussions of some case studies are followed in Sec. III, and the paper is summarized in Sec. IV.

II. THEORY MODEL

Figure 1 shows a typical model of 2D photonic crystals in the $x-y$ (or polar) system. Here, a finite number of circular cylinders with arbitrary radius are embedded arbitrarily (without overlapping) in a background material of dielectric constant ε_b. A plane wave of wave vector $\mathbf{k_0}$ ($k_0=|\mathbf{k_0}|$) illuminates the cylinders with an incident angle of α with respect to the x axis. Consider the set of N cylinders occupying a region of $\Omega=[-l,l]\times[-h,h]$, where the jth cylinder has a radius R_j, a dielectric constant $\varepsilon_j=n_j^2$ (n_j is the refractive index) and a wave number k_j. The center of the jth cylinder is $O_j(r^j,\theta^j)$ with respect to the origin O. An arbitrary point $P(r,\theta)$ outside the cylinders is described by its polar angle $\theta_j(P)$ and its distance $r_j(P)$ with respect to O_j. For the ith cylinder at O_i, (r_i^j,θ_i^j) is the relative coordinates of O_j with respect to O_i.

[a]Author to whom correspondence should be addressed: Fax: (65) 6793-3318; electronic mail: eaqliu@ntu.edu.sg

According to the 2D Fourier transformation for a limited domain, the dielectric constant of this composite system can be easily expressed as

$$\frac{1}{\varepsilon(\mathbf{x})} = \sum_{m,n=-\infty}^{\infty} D_{m,n} \exp\left[i\pi\left(\frac{mx}{l} + \frac{ny}{h}\right)\right] + \frac{1}{\varepsilon_b}, \tag{1a}$$

where m and n are integers, $i=\sqrt{-1}$, and $\mathbf{x}=x\hat{\mathbf{x}}+y\hat{\mathbf{y}}$, with $\hat{\mathbf{x}}$ and $\hat{\mathbf{y}}$ which are the unit vectors along x and y axes, respectively. Here $D_{m,n}$ is of integral form,

$$D_{m,n} = \frac{1}{4lh}\int\int_{\Omega}\sum_{j=1}^{N}\left(\frac{1}{\varepsilon_j}-\frac{1}{\varepsilon_b}\right)\exp\left[-i\pi\left(\frac{mx}{l}+\frac{ny}{h}\right)\right]dxdy$$
$$= \begin{cases} \dfrac{1}{4lh}\displaystyle\sum_{j=1}^{N}\left(\frac{1}{\varepsilon_j}-\frac{1}{\varepsilon_b}\right)\pi R_j^2 \quad (m=n=0) \\ \dfrac{1}{2lh}\displaystyle\sum_{j=1}^{N}\left(\frac{1}{\varepsilon_j}-\frac{1}{\varepsilon_b}\right)\dfrac{R_j J_1\left[\pi R_j\sqrt{\left(\frac{n}{h}\right)^2+\left(\frac{m}{l}\right)^2}\right]}{\sqrt{\left(\frac{n}{h}\right)^2+\left(\frac{m}{l}\right)^2}}\exp\left[-i\pi\left(\frac{m}{l}x^j+\frac{n}{h}y^j\right)\right] \quad (\text{others}), \end{cases} \tag{1b}$$

where $J_1(x)$ is a Bessel function, and $x^j=r^j\cos\theta^j$ and $y^j=r^j\sin\theta^j$. Equation (1) is derived in detail in Appendix A.

For an infinite periodic photonic lattice, the discrete translational symmetry of a photonic crystal allows us to classify the electromagnetic modes with a wave vector k in terms of Bloch wave. However, for a finite-size and disordered lattice, the periodicity is destructed, which prevents us from describing the modes of the system with real wave vector k. Instead, a complex wave vector, such as an effective propagation constant K is proposed.

The propagation of electromagnetic fields through random media is well studied.[12–16] Many field models were brought forward to analyze the field interactions with the individual discontinuities, such as the effective field approximation (EFA or Foldy's approximation) for low-density media and the quasicrystalline approximation (QCA) or the quasicrystalline approximation with coherent potential (QCA-CP) for higher density media. Different from the Monte Carlo approach, these field models tried to do some ensemble averaging to calculate the average (coherent) field. In particular, Twersky[16] has derived a 2D formula for calculating the effective propagation constant K,

$$K^2 = k_0^2 - 4if(\mathbf{i},\mathbf{i})\rho + [2\rho/(k_0\cos\alpha)]^2 \times\{[f(\mathbf{i}',\mathbf{i}')]^2 - [f(\mathbf{i},\mathbf{i})]^2\}, \tag{2}$$

where k_0 is the wave number of the background medium and f is the scattering field amplitude. The term $f(\mathbf{o},\mathbf{i})$ represents the amplitude, phase, and polarization of the scattered wave of far field in the direction $\mathbf{o}$ when the 2D system of cylinders is illuminated by a plane wave propagating in the direction $\mathbf{i}$ with unit amplitude. Here $\mathbf{i}'$ is the image of $\mathbf{i}$ in the plane $x=0$ (see Fig. 1) and ρ is the number density, which is defined as the number of scatterers per unit area. Actually the effective propagation constant K is a statistic result for the ensemble average, which can be used to replace the 2D system by a homogeneous effective medium. Additionally K is correct to $O(\rho^3)$, i.e., the higher-order terms can be neglected at small ρ^3.

For a finite number of arbitrary set of parallel cylinders, the scattered field at point P outside the circular cylinders can be expanded by using the scattering matrix method[5] into the Fourier-Bessel series as

$$\Psi(P) = \sum_{j=1}^{N}\sum_{m=-\infty}^{\infty} b_{j,m} H_m^{(1)}[k_0 r_j(P)]\exp[im\theta_j(P)], \tag{3}$$

where $H_m^{(1)}$ is the mth-order Hankel function of the first kind, corresponding to the time-dependent function $\exp(-i\omega t)$, and $b_{j,m}$ denotes the components of an infinite column matrix $\hat{\mathbf{b}}_j$, which can be obtained by solving the following matrix equation:

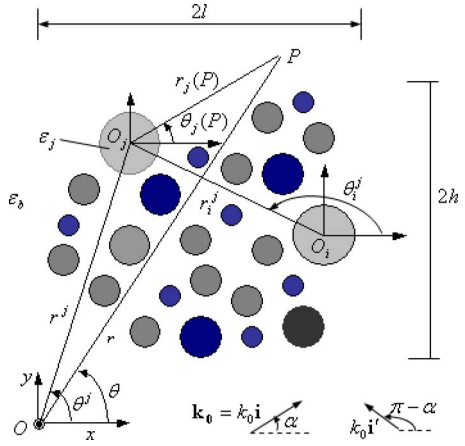

FIG. 1. Sketch for arbitrary set of parallel circular cylinders.

$$\hat{\mathbf{b}}_{\mathbf{j}} - \sum_{l \neq j} \mathbf{S}_{j,l} \mathbf{T}_{j,l} \hat{\mathbf{b}}_l = \mathbf{S}_{j,j} \mathbf{Q}_j, \tag{4a}$$

where

$$\mathbf{Q}_j = [Q_{j,m}] = \lfloor i^m \exp[ik_0 r^j \cos(\alpha - \theta^j) - im\alpha] \rfloor, \tag{4b}$$

$$\mathbf{T}_{j,l} = [T_{j,l,m,q}] = \lfloor \exp[i(q-m)\theta_j^l] H_{m-q}^{(1)}(k_0 r_j^l) \rfloor, \tag{4c}$$

$$\mathbf{S}_{j,l} = [S_{j,l,m}] = \left[-\frac{n_j J_m'(k_0 R_l) J_m(k_j R_j) - \eta J_m(k_0 R_l) J_m'(k_j R_j)}{n_j H_m^{(1)'}(k_0 R_j) J_m(k_j R_j) - \eta H_m^{(1)}(k_0 R_j) J_m'(k_j R_j)} \right], \tag{4d}$$

$$\eta = \begin{cases} 1 & \text{for } H \text{ polarization} \\ n_j^2 & \text{for } E \text{ polarization,} \end{cases} \tag{4e}$$

where $H_m^{(1)'}$ is the derivative of the Hankel function, and J_m and J_m' are the Bessel function of the first kind and its derivative, respectively.

For brevity, Eq. (4a) is written as[6]

$$\mathbf{S}^{-1}\mathbf{b} = \mathbf{a}, \tag{4f}$$

where $\mathbf{S}$ is the scattering matrix. The resonant modes of the set of cylinders are defined as solutions of Maxwell's equations without any incident field, i.e., the solutions of $\mathbf{S}^{-1}\mathbf{b} = \mathbf{0}$, which means that there exist the poles of the $\mathbf{S}$ matrix.

For numerical purposes it is clear that the series in Eq. (3) has to be truncated. Because of the properties of the Hankel function, the terms of the series are decreasing extremely fast. Assuming that M terms in the infinite series are kept, the value of M is closely linked with the radius R_j and the wavelength λ. A convenient value for M is given by the empirical rule of $M \approx 40R_j/\lambda$.[6] It was verified that the summation with respect to m in Eq. (3) may be from −2 to 2 or from −3 to 3 without increasing the error larger than 1% at PBG frequencies.[6,17] In the case study (see below), $M=7$ is used to achieve enough accuracy and a short computation time.

Using Graf's formula[18] for the Hankel function in Eq. (3) at $r \geqslant r^j$, we have

$$H_m^{(1)}[k_0 r_j(P)] \exp[im\theta_j(P)] = \sum_{q=-\infty}^{\infty} \exp[i(m-q)\theta^j] J_{q-m}(k_0 r^j) H_q^{(1)}(k_0 r) \exp(iq\theta). \tag{5a}$$

At far field, the asymptotic form of Hankel function is

$$H_m^{(1)}(kr) \approx \sqrt{2/\pi kr} \exp[i(kr - m\pi/2 - \pi/4)], \tag{5b}$$

and the scattered waves satisfy

$$\Psi \sim \sqrt{2/\pi kr} f(\mathbf{o},\mathbf{i}) \exp(ikr - i\pi/4) \quad \text{as } r \to \infty, \tag{5c}$$

therefore $f(\mathbf{i},\mathbf{i})$ can be obtained from Eqs. (3) and (5), which is

$$f(\mathbf{i},\mathbf{i}) = \sum_{j=1}^{N} \sum_{m=-\infty}^{\infty} \sum_{q=-\infty}^{\infty} b_{j,m} \exp[i(m-q)\theta^j] J_{q-m}(k_0 r^j) \times \exp\left[iq\left(\alpha - \frac{\pi}{2}\right)\right]. \tag{6}$$

In general, $f(\mathbf{i},\mathbf{i})$ is a complex number even for lossless cylinders, which means that the propagation wave attenuates through these cylinders due to the multiple scattering among them. Therefore, the propagation constant K in Eq. (2) is also a complex number.

In the cases of H polarization and E polarization, $H_z(\mathbf{x},\mathbf{K})$ and $E_z(\mathbf{x},\mathbf{K})$ can be expanded into, respectively,

$$H_z(\mathbf{x},\omega) = \sum_{m,n=-\infty}^{\infty} A(\mathbf{K}|\mathbf{G}) \exp[i(\mathbf{K}+\mathbf{G})\cdot\mathbf{x}], \tag{7}$$

$$E_z(\mathbf{x},\omega) = \sum_{m,n=-\infty}^{\infty} B(\mathbf{K}|\mathbf{G}) \exp[i(\mathbf{K}+\mathbf{G})\cdot\mathbf{x}], \tag{8}$$

where $\mathbf{K} = K\cos\alpha\hat{\mathbf{x}} + K\sin\alpha\hat{\mathbf{y}}$ is the 2D complex wave vector and $\mathbf{G} = G_x\hat{\mathbf{x}} + G_y\hat{\mathbf{y}} = \pi m/l\hat{\mathbf{x}} + \pi n/h\hat{\mathbf{y}}$.

By substituting these expansions into Maxwell's equations, two standard eigenvalue problems for the coefficients $A(\mathbf{K}|\mathbf{G})$ and $B(\mathbf{K}|\mathbf{G})$ were obtained, respectively,

$$\sum_{m',n'} (\mathbf{K}+\mathbf{G})\cdot(\mathbf{K}+\mathbf{G}') F_{m-m',n-n'} A(\mathbf{K}|\mathbf{G}') = \frac{\omega^2}{c^2} A(\mathbf{K}|\mathbf{G}), \tag{9}$$

$$\sum_{m',n'} F_{m-m',n-n'} |\mathbf{K}+\mathbf{G}'|^2 B(\mathbf{K}|\mathbf{G}') = \frac{\omega^2}{c^2} B(\mathbf{K}|\mathbf{G}), \tag{10}$$

where c is the speed of light in vacuum and $F_{m,n} = D_{m,n}$ [see Eq. (1b)] except for $F_{m,n} = D_{m,n} + 1/\varepsilon_b$ when $m=n=0$.

The eigenvalue problems posed by Eqs. (9) and (10) have an analogy to their counterparts as reported in Ref. 2. Here $\mathbf{G}$ has an analogy to the reciprocal lattice vectors in a perfectly periodic crystal. This implies that the 2D finite-size arbitrary structure can be considered as a supercell that is periodically positioned in space. However, the "supercell" here is essentially different from that of the conventional supercell method,[19,20] which is employed to deal with an infinite periodic system with some defects or a perturbational quasiperiodic structure. In the conventional supercell method, the wave vector is still a real number and the size of the supercell has to be large enough to guarantee negligible coupling between neighboring supercells. Another analogy is between the complex wave vector $\mathbf{K}$ and Bloch wave vector $\mathbf{k}$, for which the former describes localized evanescent modes of the finite crystal, and the latter is for the extended modes of the ideal and infinite crystal.

In general, any dispersive materials may be considered, whose $F_{m,n}$ and $\mathbf{K}$ in Eqs. (9) and (10) are both frequency dependent. Consequently it is invalid to solve eigenfrequencies for a given wave vector from the two eigenvalue equa-

tions. By using a revised PWM,[21] the general eigenvalue equations can be obtained for H polarization and E polarization, respectively,

$$\begin{bmatrix} [G_y] & i\omega/c + (ic/\omega)(K_x + [G_x])[F_{mn}](K_x + [G_x]) \\ i\omega/c[F_{mn}]^{-1} & [G_y] \end{bmatrix} \times \begin{bmatrix} [A_1] \\ [A] \end{bmatrix} = -K_y \begin{bmatrix} [A_1] \\ [A] \end{bmatrix}, \tag{11}$$

$$\begin{bmatrix} -[G_y] & i\omega/c[F_{mn}]^{-1} + ic/\omega(K_x + [G_x])^2 \\ i\omega/c & -[G_y] \end{bmatrix} \begin{bmatrix} [A_2] \\ [B] \end{bmatrix} = K_y \begin{bmatrix} [A_2] \\ [B] \end{bmatrix}, \tag{12}$$

where $[A_1]$ and $[A_2]$ are vectors constructed by the Fourier expansion coefficients of the field components E_x and H_x, respectively. It is obvious that the eigenvalue equations (9) and (10) are the special cases of Eqs. (11) and (12).

For a finite-size crystal with all kinds of defects arbitrarily embedded, the concept of band structure is also employed to determine whether a certain frequency will support extended states inside the crystal. As mentioned above, the absolute band gap is not necessary for the realistic crystal, and some precision in calculation is adopted to get the band structure. Because of the complex wave vector **K**, the corresponding eigenfrequencies are also complex numbers. In this case, there should be four kinds of band structures, i.e., real and imaginary **K** versus real and imaginary eigenfrequencies, respectively. Here, only the band structure of real **K** versus real eigenfrequencies is presented. On the other hand, the concept of the DOS is still valid and useful for finite and disordered structures, which defines the number of allowed states (real **K** vectors here) per unit increase in frequency. Recently, a simple definition of the electromagnetic density of modes for a finite-size structure was presented in Ref. 9, which was based on the Green's function for a generic three-dimensional open cavity filled with a linear, isotropic, dielectric material. In addition to the conventional DOS, some density of states functions were introduced,[10] including the mutual density of states (MDOS), the local density of states (LDOS), and the spectral density of states (SDOS), which give position and angular information for emission of radiation from photonic crystals. Based on scattering theory, reciprocal density of states was developed to play the role of the classical LDOS for finite structure.[11] Note that the band structure provides only the information of the gap, but it does not provide the information on how many states can be on the frequency. The examination of the DOS will allow one to obtain some additional information about the effect of disorder.

III. RESULTS AND DISCUSSIONS

In this section, some examples are given to calculate the band diagram for 2D finite-size structures by applying the method presented above. In the calculation, the admittable precision for a band gap is 0.005 (i.e., −46 dB), and 441 $\times$ 121 plane waves are used, and the computational error was estimated to be less than 1%, compared with the classical PWM.[2,22]

Figure 2(a) shows the comparison of the photonic band structure and DOS for the case of E polarization at the normal incidence between a realistic crystal with 11×11 cylinders [shown in Fig. 2(b)] and the corresponding perfect crystal. Here, $\varepsilon_a = 8.9$, $\varepsilon_b = 1$, $2l = 2h = 11a$, and the radius of cylinder $r = 0.2a = R_c$, where a is the lattice constant, and R_c is the radius of the center cylinder. Because of the symmetry, only three directions ($\Gamma - X$, $X - M$, and $M - \Gamma$) are necessarily considered. The photonic band structure shows the relationship between the wave vector $\mathbf{k}_0$ of the background medium and the normalized real frequency $\mathrm{Re}(\omega)a/2\pi c$. Given a wave vector $\mathbf{k}_0$ inside the first Brillouin zone [shown in Fig. 2(c)], the corresponding **K** vector can be figured out from Eq. (2). Then by solving the standard eigenvalue equations (9) and (10) and taking the real part of the complex eigenfrequencies, we can construct the band diagram. Along the right-hand margin of this figure we have plotted the density of photonic states in arbitrary units. Since the DOS is defined as the number of states (**K** vectors) corresponding to a frequency, this requires the Brillouin zone sampled uniformly and densely. By uniformly sampling the first Brillouin zone into $101 \times 101 = 10\,201$ spaced values of $\mathbf{k}_0$, all the corresponding **K** vectors can be obtained from Eq. (2). Then taking the real part of the complex eigenfrequencies solved from Eqs. (9) and (10) at each complex **K** vector, we calculate the number of states for each frequency and obtain the DOS. Due to the finite size, the scattering on the boundary will change the propagating wave vector amplitude in different directions, as expressed in Eq. (2). So small peaks appear in the band structure and these spikes are associated with photonic states localized in the direction of the light propagation. The resonant peaks give the real part of the complex resonant frequencies and the key to the understanding of these resonances lies in the pole structure of the photonic crystal.[11,23] The scattering matrix in Eq. (4) accounts for all possible generalized modes and, whatever the angle of incidence, there is some coupling between the incident field and the scattering modes. It should be stressed that these irregularities could not be removed by using a larger structure. Indeed the peaks are due to the presence of poles of the scattering matrix that are independent of the incident field.[11] Here light scattering on the boundary plays an important role in altering evanescent states into propagating states (probably with the wave vector lying on another direction) or from one evanescent state into another evanescent state that is characterized by a lower attenuation length. This provides the physical explanation for the shape modification of the band structure and the reduction of the band gap. Figure 2(d) shows the case when the radius of the central cylinder of the sample is increased to $R_c = 0.7a$. Due to the larger defect (in size), the amplitude of these spikes is increased, and the band gap is further reduced. This will be explained through the corresponding imaginary eigenfrequencies, as shown in Fig. 4(b) later. In addition, the plot of the density of states also confirms the reduced band gap in the band structure in the frequency range in Figs. 2(a) and 2(d), respectively. It is

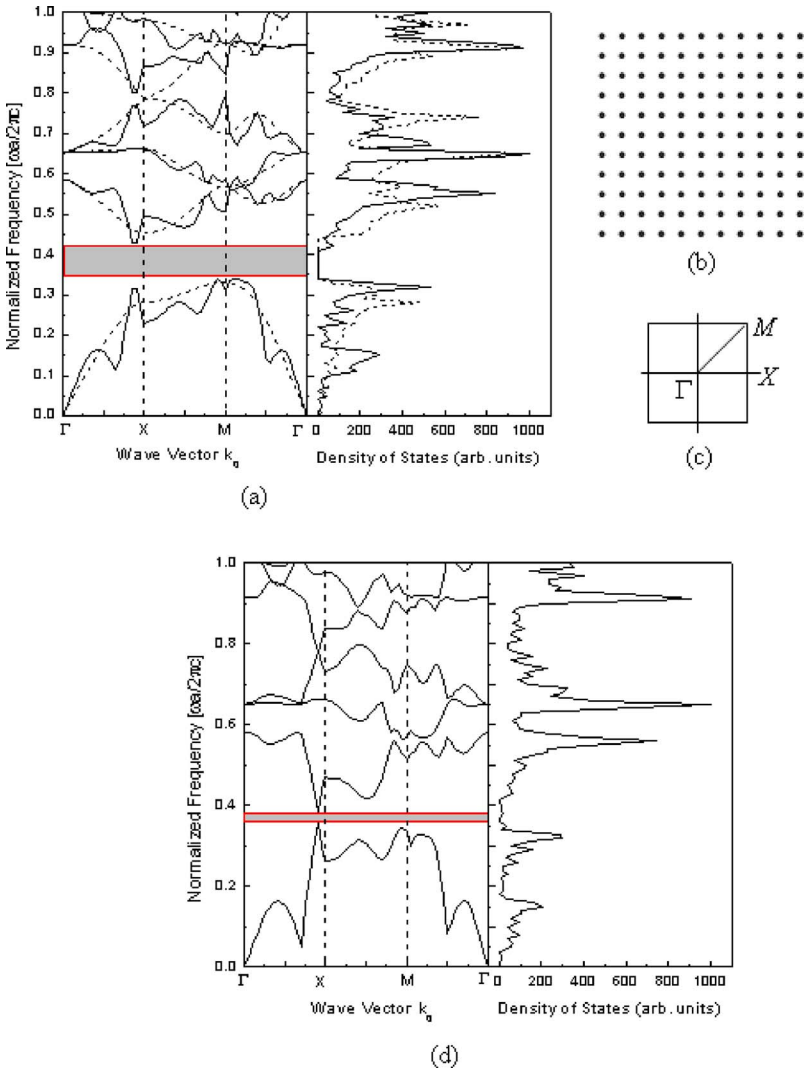

FIG. 2. (a) Comparison of the complex photonic band structure and density of states between the ideal crystal (dashed lines) and 11×11 crystal (solid lines) shown in (b), and its high-symmetry points at the corners of the Brillouin zone (c). (d) The photonic band structure and density of states for $R_c=0.7a$.

known that, for the corresponding infinite periodic crystal with a point defect, there exists a flat band—a classic indication of a defect state. Since the defect mode is isolated to the center of the lattice, its Fourier representation is not characterized by any particular direction and the same solution can be found for all parts of the Brillouin zone. However, because of the finite size, the defect state interacts with the evanescent states and propagating states, which causes the flatband to disappear as shown in Fig. 2(d).

Figure 3 shows the transmission spectra for different square lattices with $n\times n$ cylinders ($n=5$, 11, 15, 21, and 25, respectively) for E polarization at normal incidence by using the scattering matrix method, in which the shaded region defines the band gap for the corresponding infinite ideal crystal. Here the transmission ratio was defined as the flux of the Poynting vector through a segment situated near the lower face of the crystal over the flux of the Poynting vector of the incident field,[6,17] which agrees quite well with the dispersion relations in Fig. 2(a). It should be noted that this transmission ratio may be superior to 1.0.[11]

It can be seen from Fig. 3 that when n is increased from 5 to 11, the transmission inside the gap falls greatly from −25 to −53 dB, which is followed by a relatively less variation when n ranges from 15 to 25. This can be easily explained as follows: For the finite crystal, the segment used for the computation of the transmission collects a less part of the energy flowing around a larger crystal, and the falling-off tends to saturation when the crystal is large enough. Then the convergent question of the properties of the finite structure

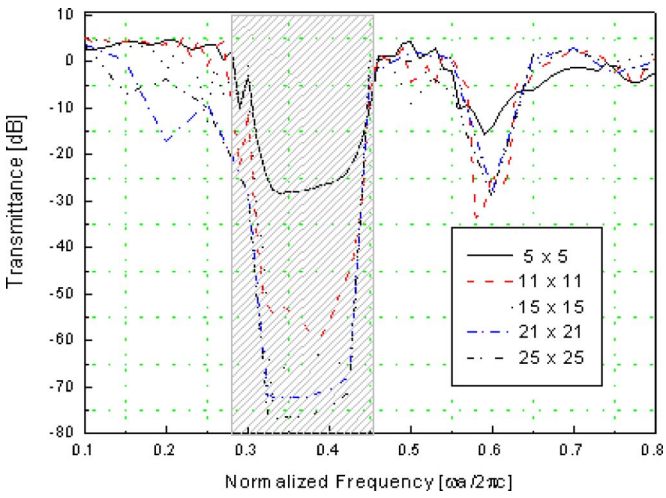

FIG. 3. (Color online) Transmission spectra for different square lattices with $n\times n$ cylinders ($n=5$, 11, 15, 21, and 25, respectively) for E polarization.

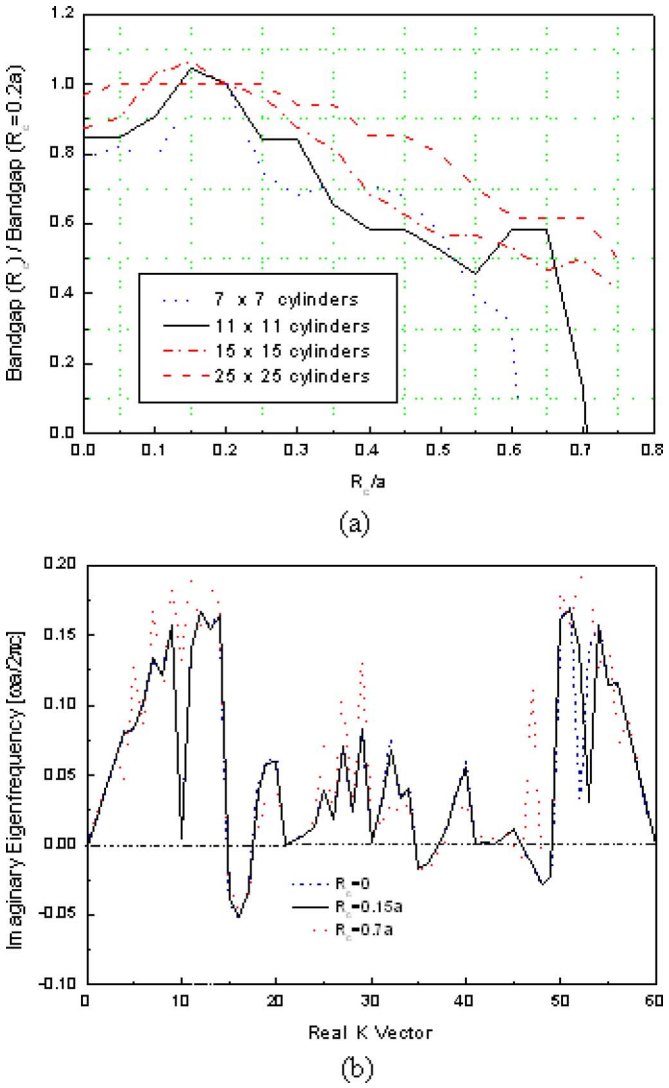

FIG. 4. (Color online) (a) The first photonic band gap for $n \times n$ cylinders with different radii of the central cylinder. (b) The real wave vector vs the imaginary eigenfrequency for the cases $R_c=0$, $0.15a$, and $0.7a$ of the 11×11 crystal.

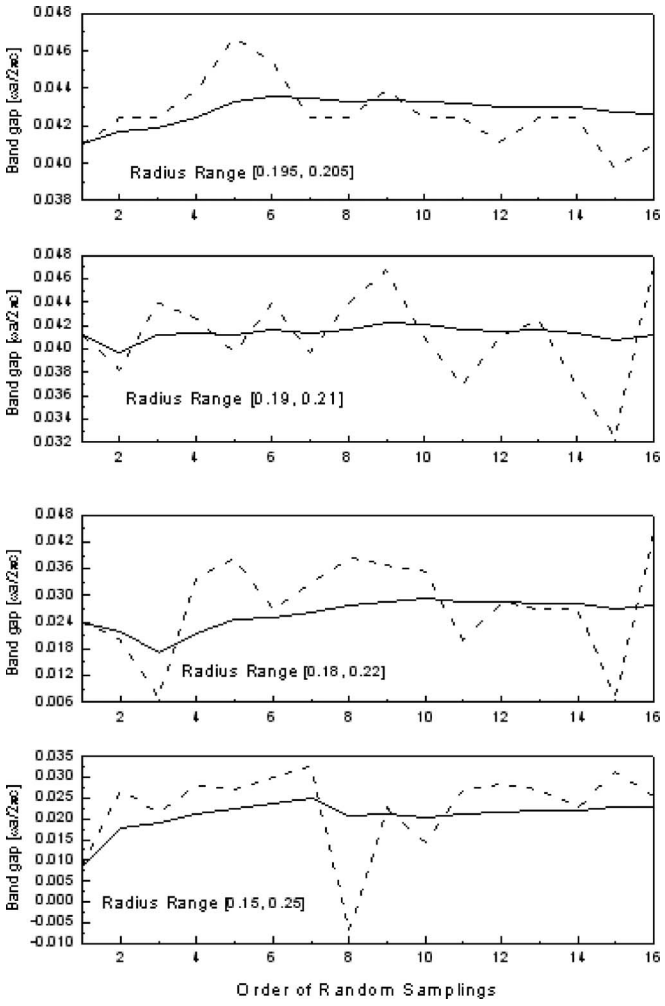

FIG. 5. Photonic band gap with random radii within different ranges, the dashed lines denote the band gap for every random sampling, and the solid lines denote the corresponding recursive average. The abscissa shows the order of the 16 random samplings.

towards that of an infinite one is posed. Felbacq and Smaâli[11] have given an excellent answer to this question, i.e., if a plane wave is used as an incident field, it is never possible to consider the finite structure as infinite because of the pole structure.

The band diagram in Fig. 2(a) is obtained for the 11×11 cylinders by the use of the above method, and the transmission spectra in the $\Gamma - X$ direction for the same crystal can also be found in Fig. 3, which are gotten by the use of the scattering matrix method. Comparing these two figures, it can be found that the first band gap in the $\Gamma - X$ direction coincides very well, in which the method presented in the paper is verified.

Figure 4(a) shows the normalized band gap (in terms of $R_c=0.2a$ case) for various $n \times n$ cylinders ($n=7$, 11, 15, and 25) with different R_c. It can be seen that the band gap is maximum (≈ 1.05) at $R_c=0.15a$ for intermediate size $n=11$ and $n=15$. For a small n ($n=7$), the maximum band gap equals to 1 at $R_c=0.2a$ as expected. For a large structure ($n=25$), a small change in defect will not affect the band gap, and the maximum band gap equals to 1 for a broad range of R_c/a ($=0.05-0.25$). The results indicate that the defect ($R_c=0.15a$) for finite 2D structures ($n=11$ and $n=15$) can increase the band gap by about 5%. This can be explained in the way that the boundaries and the defect form a resonatory cavity to localize those propagation states. This finding is different from other studies of the infinite periodic crystal,[19,20] which indicate that the nonuniform structure will reduce the band gaps. Figure 4(b) presents the relationship between the real **K** vector and the corresponding imaginary eigenfrequency for 11×11 cylinders. Considering the first photonic band gap, the imaginary eigenfrequencies among the cases $R_c=0$, $0.15a$, and $0.7a$, are compared, with the first mode shown correspondingly. The imaginary eigenfrequencies are obviously maximum (minimum) at $R_c=0.7a$ ($R_c=0.15a$). This means that a bigger evanescence at $R_c=0.7a$ will reduce the band gap significantly, which confirms the finding of the maximum band gap at $R_c=0.15a$ as shown in Fig. 4(a).

Figure 5 shows the band gaps of the photonic band diagram of real **K** vector versus real eigenfrequencies for 11×11 cylinders varied with every sampling in which every

radius of the cylinders is randomly chosen within different ranges. Here the radius of every cylinder is generated by a uniform random sampling from a finite range of radius. As shown in Fig. 5, the abscissa shows the order of the 16 random samplings, the dashed lines denote the band gap for every random sampling, and the solid lines denote the corresponding recursive average. It can be seen that the band gap is reduced when the radius range is increased on an average. This point is very useful to the fabrication process and to evaluating the effect of the surface roughness on the photonic band gap. The calculation of the photonic band diagram for a realistic disorder medium with random embedded nanostructures is currently in progress, which will be published elsewhere.

IV. CONCLUSIONS

In conclusion, a formulation has been presented to calculate the complex photonic band diagram and DOS for electromagnetic waves propagating in a 2D finite structure with nonoverlapping and nonuniform dielectric cylinders, which are arbitrarily embedded in a dielectric matrix. Complex band diagrams are numerically computed for a 2D finite and periodic square lattice with a defect at the center. The simulation result shows that an optimal size of a defect at the center of a finite-size photonic crystal can increase the photonic band gap. The studies of this approach for more complicated structures with arbitrary defects will be reported elsewhere. The potential applications of this work are expected in various disorder systems, such as random laser and random nanoparticles and nanowires in a dielectric medium.[24]

ACKNOWLEDGMENTS

The authors are grateful to Professor Kejiang Zhou from Zhejiang University for his stimulating discussions.

APPENDIX

According to the two-dimensional Fourier transformation, if any function $f(x,y)$ is integrable and absolutely integrable in the domain $\Omega=[-l,l]\times[-h,h]$, it can be expanded into the following Fourier series:

$$f(x,y)=\sum_{m,n=-\infty}^{\infty} e_{m,n}\exp[i\pi(mx/l+ny/h)], \tag{A1}$$

where

$$e_{m,n}=\frac{1}{4lh}\int\int_{\Omega} f(x,y)\exp\left[-i\pi\left(\frac{mx}{l}+\frac{ny}{h}\right)\right]dxdy. \tag{A2}$$

For the 2D finite-sized photonic crystal shown in Fig. 1, the dielectric constant is position dependent and can be expressed as

$$\frac{1}{\varepsilon(\mathbf{x})}=\begin{cases}1/\varepsilon_j & \text{if } \mathbf{x}\in C_j(j=1,2,\ldots,N)\\ 1/\varepsilon_b & \text{if } \mathbf{x}\notin C_j(j=1,2,\ldots,N),\end{cases} \tag{A3}$$

where C_j is the cross section of the jth cylinder.

By the use of the following integral[25]

$$J_0(\sqrt{z^2-t^2})=\frac{1}{\pi}\int_0^{\pi} e^{t\cos\theta}\cos(z\sin\theta)d\theta, \tag{A4}$$

differatiating both side of (A4) with respect to z, it can be obtained that

$$\int_0^{\pi} e^{t\cos\theta}\sin(z\sin\theta)\sin\theta d\theta=\pi z J_1(\sqrt{z^2-t^2})/\sqrt{z^2-t^2}. \tag{A5}$$

Therefore,

$$\frac{1}{\varepsilon(\mathbf{x})}-\frac{1}{\varepsilon_b}=\sum_{m,n=-\infty}^{\infty} D_{m,n}\exp\left[i\pi\left(\frac{mx}{l}+\frac{ny}{h}\right)\right], \tag{A6}$$

where

$$\begin{aligned}D_{m,n}&=\frac{1}{4lh}\int\int_{\Omega}\sum_{j=1}^{N}\left(\frac{1}{\varepsilon_j}-\frac{1}{\varepsilon_b}\right)\exp\left[-i\pi\left(\frac{mx}{l}+\frac{ny}{h}\right)\right]dxdy\\&=\frac{1}{4lh}\sum_{j=1}^{N}\left(\frac{1}{\varepsilon_j}-\frac{1}{\varepsilon_b}\right)\int\int_{C_j}\exp\left[-i\pi\left(\frac{mx}{l}+\frac{ny}{h}\right)\right]dxdy\\&=\frac{1}{4lh}\sum_{j=1}^{N}\left(\frac{1}{\varepsilon_j}-\frac{1}{\varepsilon_b}\right)\int_{x^j-R_j}^{x^j+R_j}\int_{y^j-\sqrt{R_j^2-(x^j-x)^2}}^{y^j+\sqrt{R_j^2-(x^j-x)^2}}\\&\quad\times\exp\left[-i\pi\left(\frac{mx}{l}+\frac{ny}{h}\right)\right]dxdy.\end{aligned} \tag{A7}$$

If $m=n=0$,

$$D_{m,n}=\frac{1}{4lh}\sum_{j=1}^{N}\left(\frac{1}{\varepsilon_j}-\frac{1}{\varepsilon_b}\right)\pi R_j^2, \tag{A8}$$

else

$$\begin{aligned}D_{m,n}&=\frac{1}{4lh}\sum_{j=1}^{N}\left(\frac{1}{\varepsilon_j}-\frac{1}{\varepsilon_b}\right)\frac{2\exp(-i\pi y^j n/h)}{\pi n/h}\int_{x^j-R_j}^{x^j+R_j}\exp\left(\frac{-i\pi mx}{l}\right)\sin\left[\frac{\pi n}{h}\sqrt{R_j^2-(x_j-x)^2}\right]dx\\&=\frac{1}{2lh}\sum_{j=1}^{N}\left(\frac{1}{\varepsilon_j}-\frac{1}{\varepsilon_b}\right)\exp\left[-i\pi\left(\frac{m}{l}x^j+\frac{n}{h}y^j\right)\right]\frac{1}{\pi n/h}\int_0^{\pi}\exp\left(\frac{i\pi mR_j\cos\theta}{l}\right)\sin\left(\frac{\pi n}{h}R_j\sin\theta\right)R_j\sin\theta d\theta.\end{aligned} \tag{A9}$$

By the use of Eq. (A5), there is

$$D_{m,n} = \frac{1}{2lh}\sum_{j=1}^{N}\left(\frac{1}{\varepsilon_j} - \frac{1}{\varepsilon_b}\right)\frac{R_j J_1[\pi R_j\sqrt{(n/h)^2 + (m/l)^2}]}{\sqrt{(n/h)^2 + (m/l)^2}}\exp\left[-i\pi\left(\frac{m}{l}x^j + \frac{n}{h}y^j\right)\right]. \tag{A10}$$

Therefore Eqs. (1a) and (1b) in the text are obtained.

[1] J. D. Joannopoulos, R. D. Meade, and J. N. Winn, *Photonic Crystals: Molding the Flow of Light* (Princeton University Press, Princeton, NJ, 1995).
[2] M. Plihal and A. A. Maradudin, Phys. Rev. B **44**, 8565 (1991).
[3] A. Mekis, J. C. Chen, I. Kurland, S. Fan, P. R. Villeneuve, and J. D. Joannopoulos, Phys. Rev. Lett. **77**, 3787 (1996).
[4] N. Garcia, E. V. Ponizovskaya, H. Zhu, J. Q. Xiao, and P. Pons, Appl. Phys. Lett. **82**, 3147 (2003).
[5] D. Felbacq, G. Tayeb, and D. Maystre, J. Opt. Soc. Am. A **11**, 2526 (1994).
[6] G. Tayeb and D. Maystre, J. Opt. Soc. Am. A **14**, 3323 (1997).
[7] W. M. Robertson, G. Arjavalingam, R. D. Meade, K. D. Brommer, A. M. Rappe, and J. D. Joannopoulos, Phys. Rev. Lett. **68**, 2023 (1992).
[8] Z.-Y. Li and L.-L. Lin, Phys. Rev. E **67**, 046607 (2003).
[9] G. D'Aguanno, N. Mattiucci, M. Centini, M. Scalora, and M. J. Bloemer, Phys. Rev. E **69**, 057601 (2004).
[10] R. C. McPhedran, L. C. Botten, J. McOrist, A. A. Asatryan, and C. M. de Sterke, Phys. Rev. E **69**, 016609 (2004).
[11] D. Felbacq and R. Smaâli, Phys. Rev. B **67**, 085105 (2003).
[12] L. Tsang and J. A. Kong, *Scattering of Electromagnetic Waves: Advanced Topics* (Wiley, New York, 2001).
[13] A. Isbimaru, *Wave Propagation and Scattering in Random Media* (IEEE, New York, 1997).
[14] L. L. Foldy, Phys. Rev. **67**, 107 (1945).
[15] M. Lax, Phys. Rev. **85**, 621 (1952).
[16] V. Twersky, J. Math. Phys. **3**, 700 (1962).
[17] J. Yonekura, M. Ikeda, and T. Baba, J. Lightwave Technol. **17**, 1500 (1999).
[18] M. Abramovitz and I. Stegun, *Handbook of Mathematical Functions* (Dover, New York, 1970).
[19] Z.-Y. Li, X. Zhang, and Z.-Q. Zhang, Phys. Rev. B **61**, 15738 (2000).
[20] H.-Y. Ryu, J.-K. Hwang, and Y.-H. Lee, Phys. Rev. B **59**, 5463 (1999).
[21] S. Shi, C. Chen, and D. W. Prather, Appl. Phys. Lett. **86**, 043104 (2005).
[22] M. Qiu and S. He, Phys. Rev. B **60**, 10610 (1999).
[23] E. Centeno and D. Felbacq, J. Opt. Soc. Am. A **16**, 2705 (1999).
[24] N. Garcia, E. V. Ponizovskaya, and J. Q. Xiao, Appl. Phys. Lett. **80**, 1120 (2002).
[25] Z. X. Wang, and D. R. Guo, *Special Functions* (World Scientific, Singapore, 1989).